Published in final edited form as:
J Am Chem Soc. 2010 April 28; 132(16): 5906–5915. doi:10.1021/ja1014103.

A Palette of Fluorescent Probes with Varying Emission Colors for Imaging Hydrogen Peroxide Signaling in Living Cells

Bryan C. Dickinson[1], **Calvin Huynh**[1], and **Christopher J. Chang**[1,2]
Christopher J. Chang: chrischang@berkeley.edu
[1]Department of Chemistry, University of California, Berkeley, CA 94720, USA
[2]Howard Hughes Medical Institute, University of California, Berkeley, CA 94720, USA

Abstract

We present a new family of fluorescent probes with varying emission colors for selectively imaging hydrogen peroxide (H_2O_2) generated at physiological cell signaling levels. This structurally homologous series of fluorescein- and rhodol-based reporters relies on a chemospecific boronate-to-phenol switch to respond to H_2O_2 over a panel of biologically relevant reactive oxygen species (ROS) with tunable excitation and emission maxima and sensitivity to endogenously produced H_2O_2 signals, as shown by studies in RAW 264.7 macrophages during the phagocytic respiratory burst and A431 cells in response to EGF stimulation. We further demonstrate the utility of these reagents in multicolor imaging experiments by using one of the new H_2O_2-specific probes, Peroxy Orange 1 (PO1), in conjunction with the green-fluorescent highly reactive oxygen species (hROS) probe, APF. This dual-probe approach allows for selective discrimination between changes in H_2O_2 and hypochlorous acid (HOCl) levels in live RAW 264.7 macrophages. Moreover, when macrophages labeled with both PO1 and APF were stimulated to induce an immune response, we discovered three distinct types of phagosomes: those that generated mainly hROS, those that produced mainly H_2O_2, and those that possessed both types of ROS. The ability to monitor multiple ROS fluxes simultaneously using a palette of different colored fluorescent probes opens new opporunities to disentangle the complex contributions of oxidation biology to living systems by molecular imaging.

Introduction

The production of reactive oxygen species (ROS) molecules by biological systems is an inevitable consequence of aerobic life.[1,2] The mismanagement and accumulation of ROS in mammals leads to a condition broadly referred to as oxidative stress, in which the production and destruction of the various cellular oxidants no longer maintains a healthy equilibrium.[3] Oxidative stress is linked to aging and a host of diseases where age is a risk factor, including cancer[4–6] and neurodegenerative Alzheimer's and Parkinson's diseases.[6–8] However, whereas ROS can be damaging when uncontrolled, they also have the potential to be used for beneficial biological activities ranging from immune response to cell signaling.[9–20] At the cellular level, the delicate balance between oxidative stress and signaling is influenced by the chemistry of a particular ROS or set of ROS, as they are not generated in isolation of one another and can often interconvert and undergo further reactions to produce other ROS metabolites.[3,18,21,22] In other words, at any given time a cell is producing a variety of ROS, where each type exerts specific downstream biological effects. As the lifetimes and reactivities of individual classes

Correspondence to: Christopher J. Chang, chrischang@berkeley.edu.

Supporting Information Available: Additional imaging data. This information is available free of charge via the Internet at http://pubs.acs.org.

of ROS can greatly vary,[18] studying multiple ROS simultaneously in a single cell is critical to understanding their discrete roles in complex environments.

Fluorescent probes are well suited to study the generation of specific types of ROS in biological systems, as optical microscopy allows for the use of multiple probes simultaneously in a single specimen as long as spectral overlap is sufficiently minimized.[23–29] In this regard, several new types of indicators have been reported for detection of nitric oxide (NO),[15,30–36] peroxynitrite,[37,38] and nitrative stress,[39] as well as superoxide,[40–43] singlet oxygen,[44,45] ozone,[46] H_2O_2,[16,47–65] hypochlorous acid,[66,67] highly reactive oxygen species (hROS),[68–70] and general redox events.[71–84] In terms of H_2O_2 detection, we previously described the design, synthesis, and characterization of Peroxyfluor-1 (PF1, Scheme 1),[51] a novel probe for H_2O_2 in which two H_2O_2-mediated boronate deprotections yields the highly fluorescent dye molecule fluorescein. Owing to its chemospecific deprotection mechanism, PF1 and related bisboronate derivatives exhibit high selectivity for H_2O_2 over other ROS and can respond to changes in H_2O_2 fluxes at oxidative stress levels.[53,58,62] To maintain H_2O_2 specificity while increasing sensitivity to image H_2O_2 produced at low signaling levels, we devised the single boronate caged probes Peroxy Green 1 (PG1, Scheme 1) and Peroxy Crimson 1 (PC1, Scheme 1).[16] Green-fluorescent PG1 was capable of visualizing endogenous H_2O_2 generation in both A431 cells and primary neurons upon epidermal growth factor (EGF) stimulation, but red-fluorescent PC1 was not responsive enough detect peroxide bursts at these basal levels. Because the most common types of fluorescent reporters utilize GFP, fluorescein, or related green-colored fluorophores that overlap and are thus incompatible with PG1 for multicolor imaging experiments, we sought to address this shortcoming by expanding the available palette of colors for chemospecific peroxide imaging at low cell signaling levels. We now report a new series of monoboronate probes that responds to H_2O_2 over a range of rationally tunable visible excitation and emission wavelengths (Scheme 1). Three of these derivatives, Peroxyfluor-3 (PF3), Peroxy Yellow 1 (PY1), and Peroxy Orange 1 (PO1), are sensitive enough to image H_2O_2 signals produced in RAW 264.7 macrophages and A431 cells during immune response and growth factor stimulation, respectively. Moreover, dual-color imaging experiments using PO1 along with the green-fluorescent highly reactive oxygen species (hROS) probe APF allows for selective discrimination between changes in H_2O_2 and hypochlorous acid (HOCl) levels in macrophages, as well as identification of phagosomes that produce H_2O_2 and/or hROS during endogenous immune response.

Results and Discussion

Design and Synthesis of a Palette of Monoboronate Fluorescent Probes for Hydrogen Peroxide Based on Fluorescein and Rhodol Scaffolds

The original Tokyo Green fluorophore scaffold utilized for PG1, although functional in many ways, is limited to green emission profiles. We therefore turned our attention to fluorescein and rhodol dyes that allow us to rationally expand the palette of excitation and emission colors throughout the visible region by altering oxygen or nitrogen substituents on the 2' position of the xanthene core (Scheme 1). Scheme 2 and Scheme 3 outline synthetic routes to a family of five new monoboronate probes for chemoselective H_2O_2 detection. Two of these probes are based on green methoxyfluorescein (Peroxyfluor-2, PF2) and fluorescein (Peroxyfluor-3, PF3) platforms, whereas the other three reporters feature rhodol derivatives made from aminophenol (Peroxy Emerald 1, PE1), diethylaminophenol (Peroxy Yellow 1, PY1), and julolidine (Peroxy Orange 1, PO1) building blocks. Briefly, treatment of the parent dyes with *N*-phenyl bis (trifluoromethanesulfonamide) affords the corresponding triflate derivatives, and palladium-mediated coupling with bis(pinacolato)diboron furnishes the final boronate-protected products. PF3 was then acetylated with acetic anhydride to yield PF3-Ac in order to increase cell permeability, where the acetyl functionality should be removed by non-specific esterases

once inside the cytoplasm to reveal PF3. We anticipate that this modular synthetic strategy should be applicable to a wide variety of scaffolds and note complementary synthetic methods for C-N and C-O bond formation that have been reported in the recent literature,[85–92] as well as a triphenylphosphonium-capped piperazine rhodol for mitochondrial targeting.61

Spectroscopic Properties and Responses to Hydrogen Peroxide

We evaluated the spectral properties and H_2O_2 responses of the new monoboronate dyes in aqueous media buffered to physiological pH (20 mM HEPES buffer, pH 7); data are provided in Table 1. The methoxy and boronate groups on PF2 force it to adopt a closed lactone form that is nonfluorescent and displays no absorption features in the visible region. The other four dyes each feature one prominent absorbance band in the visible region with weak but measurable fluorescence. The addition of H_2O_2 triggers a marked increase in fluorescence intensity for all five probes (Figure 1, S1) with available emission colors spanning from green to yellow to orange. As expected because of their common boronate switch, the fluorescein and rhodol reporters respond with good selectivity to H_2O_2 over a variety of biologically relevant ROS, including superoxide, NO, hypochlorite, and *tert*-butyl hydroperoxide, as well as hydroxyl and *tert*-butoxy radicals (Figure 2). Kinetics measurements of the H_2O_2-mediated boronate deprotections were performed under pseudo-first-order conditions (5 μM dye, 10 mM H_2O_2), giving observed rate constants ranging from $k = 3.7(1)$ to $8.2(1) \times 10^{-3}$ s^{-1}. These data provide further evidence that H_2O_2-triggered conversion of boronates to phenols is a robust and versatile methodology for reaction-based H_2O_2 detection.

Fluorescence Detection of H_2O_2 in Living Cells in Situations of Oxidative Stress

With data establishing that all five monoboronate reporters selectively respond to H_2O_2 in aqueous solution, we turned our attention to assessing their performance in live-cell imaging assays. Incubation of live A431 cells with 10 μM PF2, 5 μM PF3-Ac, 5 μM PY1, or 5 μM PO1 for 40 min at 37 °C results in low levels of intracellular fluorescence as determined by scanning confocal microscopy measurements (Figure 3a,d,g,j), and addition of 100 μM H_2O_2 to these dye-loaded cells for 20 min at 37 °C triggers increases in green, yellow, or orange intracellular fluorescence (Figure 3b,e,h,k). PE1 does not show a turn-on response to H_2O_2 in cells under similar conditions owing to high background staining. Further bright field transmission and nuclear staining experiments confirm that the cells are viable throughout the imaging assays (Figures S2, S3). These experiments demonstrate that four of the probes, PF2, PF3-Ac, PY1, and PO1, are cell-permeable, non-toxic, and capable of detecting elevations in H_2O_2 levels under oxidative stress conditions. The excitation wavelengths of this series of reagents align well with the 488 nm (PF2, PF3-Ac), 514 nm (PY1), and 543 nm (PO1) laser lines commonly used for light microscopy.

Fluorescence Detection of H_2O_2 at Signaling Levels Upon Immune or Growth Factor Stimulation

We next tested whether the monoboronate probes were sensitive enough to detect H_2O_2 produced at low signaling levels upon physiological stimulation. Initial experiments focused on macrophages, which fight off infections by engulfing pathogens and using NADPH oxidase (Nox) and associated proteins to produce H_2O_2 and other ROS to alleviate the threat.[12,18] We utilized RAW264.7 macrophages, which are estimated to produce low micromolar levels of H_2O_2 upon stimulation with phorbol myristate acetate (PMA),[93–95] as a cell line model for H_2O_2-mediated immune response. RAW264.7 cells loaded with 10 μM PF2, 5 μM PF3-Ac, 5 μM PY1, or 5 μM PO1 for 60 min at 37 °C show low levels of intracellular fluorescence (Figure 4a,e,i,m). Upon stimulation of probe-loaded cells with PMA for 40 min at 37 °C to induce an immune response, we observe bright, punctate fluorescent patterns corresponding to phagocytic vesicles (Figure 4b,f,j,n), showing that these reporters can visualize endogenous

production of H_2O_2 under conditions of immune signaling. We confirmed cell viability during live-cell imaging using a combination of brightfield transmission and nuclear staining experiments (Figures S4, S5).

We then sought to expand the utility of these fluorescent indicators to image H_2O_2 signaling in non-phagocytic systems. In particular, mounting data reveals that Nox proteins used in phagocytic ROS killing are also expressed in a wide variety of non-phagocytic cell types throughout the body, and that these enzyme complexes can be activated by ligands such as growth factors and cytokines. We previously showed that A431 cells, which express high levels of epidermal growth factor receptor (EGFr), respond to epidermal growth factor (EGF) stimulation by producing H_2O_2 via a Nox/PI3K pathway.[16] Along these lines, A431 cells loaded with 5 μM PF3-Ac, 5 μM PY1, or 5 μM PO1 for 60 min at 37 °C display modest intracellular fluorescence (Figure 5a,d,g). Treatment of the dye-loaded cells with 500 ng/mL EGF ligand for 40 min at 37 °C triggers a modest turn-on enhancement in bright green, yellow, or orange intracellular fluorescence compared to unstimulated cells (Figure 5b,e,h) via Nox-generated H_2O_2. Brightfield transmission and nuclear staining measurements confirm that the cells are viable throughout the imaging experiments (Figures S6, S7). Taken together, PF3-Ac, PY1, and PO1 offer a set of green, yellow, and orange dyes that are capable of detecting endogenous bursts of H_2O_2 produced for physiological signaling purposes.

Simultaneous, Dual-Color Imaging of H_2O_2 and hROS in Living Cells with Complementary Chemoselective Fluorescent Probes

Our next goal was to exploit the utility of the newly developed H_2O_2-specific fluorescent indicators with varying emission profiles to image multiple analytes/processes in living cells. In particular, because a given ROS can undergo an array of primary and secondary reactions to produce other classes of ROS molecules, we envisioned using a dual-probe approach to simultaneously visualize H_2O_2 and an additional important downstream product of cellular H_2O_2 chemistry. We focused on macrophages as a cell model system, as H_2O_2 produced by Nox complexes in these cell types can be converted to HOCl by reaction with heme-dependent myeloperoxidase enzymes.[96–99] For dual-color imaging experiments, we selected APF,[68] a 4-aminophenyl-fluorescein reporter developed by Nagano and co-workers that responds selectively to HOCl and other highly reactive oxygen species (hROS) by an increase in green fluorescence (488 nm excitation, 520 nm emission), along with the H_2O_2-selective probe PO1 that responds in a complementary orange optical window (543 nm excitation, 565 nm emission).

Initial experiments sought to test the ROS specificities of these dyes in a dual-probe/dual-color imaging mode. To this end, RAW264.7 macrophages loaded simultaneously with 5 μM APF and 5 μM PO1 for 50 min at 37 °C display low levels of both green and orange fluorescence (Figure 6a,b). In contrast, APF- and PO1-stained cells incubated with 50 μM H_2O_2 for 20 min exhibit a selective increase in intracellular orange fluorescence from PO1 without any change in green emission from the APF probe (Figure 6c,d). Moreover, APF- and PO1-loaded cells incubated with 100 μM HOCl for 20 min give a selective turn-on increase in intracellular green fluorescence from APF without any change in orange emission from the PO1 dye (Figure 6e,f). In all cases, brightfield transmission and nuclear staining measurements confirm reasonable cell viability through the duration of the imaging assays (Figure S8), however the exogenous ROS treatments can cause some toxicity. This set of experiments establishes not only that fluorescence signals arising from green APF and orange PO1 probes can be distinguished by optical microscopy, but also that each reporter maintains its chemical selectivity in the presence of one another in living systems.

We then moved on to study endogenously produced ROS bursts using this dual-probe imaging approach. APF- and PO1-loaded macrophages stimulated with 1 μg/mL PMA for 20 min

display bright, punctate patterns of green and/or orange fluorescence localized to phagosomes, where ROS are generated in response to immune insult (Figure 6g,h, S8). As shown in Figure 7 and Figure S9, we discovered three classes of phagosomes that are characterized by different relative ratios of H_2O_2 and hROS fluxes. Specifically, some phagosomes display only PO1-derived orange fluorescence, indicating that H_2O_2 production dominates (Figure 7a,b,c,d), whereas other phagosomes show only APF-derived green fluorescence, indicating that most of the phagocytic burst results in formation of hROS (Figure 7e,f,g,h). A third distinct class of phagosomes possesses both green and orange fluorescence signals (Figure 7i,j,k,l) resulting from a combination of phagocytic increases in both H_2O_2 and hROS. These data establish that the dual-probe approach can reveal chemical differences through simultaneous imaging of discrete classes of ROS molecules.

Concluding Remarks

To close, we have described the synthesis, properties, and biological applications of a new class of monoboronate fluorescent probes for imaging H_2O_2 produced at low signaling levels with a range of varying excitation and emission colors. By rationally tuning substitutents on a homologous xanthene core, we have developed boronate-caged fluorescein and rhodol derivatives for H_2O_2 detection with excitation profiles that match well with common 488 nm, 514 nm, and 543 nm lines used for light microscopy. All five probes in this series give a selective turn-on fluorescence response to H_2O_2 in aqueous solution buffered to physiological pH with minimal interference from other biologically relevant ROS. Moreover, PF2, PF3-Ac, PY1, and PO1 are capable of visualizing changes in H_2O_2 levels in living cells in situations of oxidative stress, and PF3-Ac, PY1, and PO1 can be used to image low levels of H_2O_2 produced for signaling purposes upon phagocytic immune or non-phagocytic growth factor stimulation in live samples. Owing to the expanded color palette of H_2O_2-selective probes with sensitivity to low cell signaling levels, we were able to combine one of our newly synthesized H_2O_2 probes, PO1, with a complementary green-fluorescent reporter for hROS, APF, for selective discrimination between changes in H_2O_2 and HOCl levels in live RAW 264.7 macrophages by a dual-probe/dual-color imaging approach. Further, we observed that PMA-stimulated macrophages were shown to respond with three discrete types of phagosomes via PO1/APF imaging: those that produced primarily hROS and selectively turned on APF during the phagocytic burst, those that primarily generated H_2O_2 and caused an increase in PO1 fluorescence, and those that deprotected both PO1 and APF probes and, therefore, possessed an elevated mixture of both H_2O_2 and hROS during immune signaling. By establishing selective H_2O_2-responsive probes with varying emission colors that can be used at low signaling levels, this work greatly expands our ability to study peroxide biology, particularly in conjunction with other reporters for cellular analytes and reaction processes. We are currently pursuing such opportunities in a variety of physiological and disease models, with particular interest in brain and immune systems.

Experimental Section

Synthetic Materials and Methods

All reactions were carried out under a dry nitrogen atmosphere. 2-(4-Diethylamino-2-hydroxybenzoyl)benzoic acid,100 8-Hydroxy-9-o-carboxybenzoyljulolidine, 101 rhodol,102 and methoxyfluorescein103 were synthesized according to literature methods. Silica gel P60 (SiliCycle) was used for column chromatography. Analytical thin layer chromatography was performed using SiliCycle 60 F254 silica gel (precoated sheets, 0.25 mm thick). All chemicals were purchased from Sigma-Aldrich (St. Louis, MO) and used as received. ^{1}H NMR, ^{13}C NMR, and ^{31}P NMR spectra were collected in $CDCl_3$, $(CD_3)_2O$, or 9:1 $CDCl_3/CD_3OD$ (Cambridge Isotope Laboratories, Cambridge, MA) at 25 °C on a Bruker AV-300, AVQ-400, or DRX-500 spectrometer at the College of Chemistry NMR Facility at the University of

California, Berkeley. All chemical shifts are reported in the standard δ notation of parts per million using the peak of residual solvent proton signals as an internal reference. High-resolution mass spectral analyses were carried out at the College of Chemistry Mass Spectrometry Facility at the University of California, Berkeley. Low-resolution mass spectral analyses were carried out on an Agilent 6130 LC/MS system (Santa Clara, CA). Microwave reactions were performed using a CEM Intelligent Explorer/Discover (Matthews, NC).

Methoxyfluorescein triflate (1)

Methoxyfluorescein (500 mg, 1.45 mmol) and *N*-phenyl bis(trifluoromethanesulfonamide (2.06 g, 5.78 mmol) were added to a vial and dissolved in 10 mL of dimethylformamide. Diisopropylethylamine (1.22 mL, 7.37 mmol) was then added and the reaction stirred for 120 minutes at room temperature. The reaction was then extracted into dichloromethane, washed three times with water, and dried under reduced pressure. Purification by column chromatography (2:1 hexanes/ethyl acetate) yielded **1** as a white solid (440 mg, 63%). ^{1}H NMR ($(CD_3)_2O$, 400 MHz): δ 8.0 (1H, d, *J* = 7.6 Hz), 7.84 (1H, dt, *J* = 1.2, 7.2 Hz), 7.78 (1H, dt, *J* = 1.2, 7.2 HZ), 7.54 (1H, D, *J* = 2.4 Hz), 7.38 (1H, d, *J* = 7.6 Hz), 7.25 (1H, dd, *J* = 2.4, 8.8 Hz), 7.13 (1H, d, *J* = 8.8 Hz), 7.94 (1H, d, *J* = 2.4 Hz), 6.82 (1H, d, *J* = 8.8 Hz), 6.78 (1H, dd, *J* = 2.4, 8.8 Hz), 3.89 (3H, s). ^{13}C NMR ($(CD_3)_2O$, 100 MHz): δ 169.2, 162.9, 153.6, 152.9, 152.8, 151.1, 136.6, 131.6, 131.4, 130.1, 127.3, 125.9, 125.0, 121.5, 118.1, 113.6, 111.9, 111.5. 101.73, 56.24. ^{19}F NMR ($(CD_3)_2O$, 376.5 MHz): δ-73.25. HR-FABMS: calculated for [M^+] 479.0412, found 479.0426.

Peroxyfluor-2, PF2 (2)

Compound **1** (150 mg, 0.31 mmol), Bis(pinacolato)diboron (120 mg, 0.47 mmol), Palladium acetate (63 mg, 0.10 mmol), and cyclo-hexyl JohnPhos (66 mg, 0.20 mmol) were added to a glass vial in an inert atmosphere glove box and dissolved in 3 mL of dioxane. Diisopropylethamine (0.31 mL, 1.79 mmol) was then added the vial and the contents stirred at room temperature overnight. The contents were then brought out of the box and dried under reduced pressure. Purification by column chromatography (2:1 hexanes/ethyl acetate) afforded PF2 as a white solid (103 mg, 73%). ^{1}H NMR ($(CD_3)_2O$, 400 MHz): δ8.02 (1H, d *J*=7.6 Hz), 7.79 (1H, t, *J* = 6.8 Hz), 7.74 (1H, t, *J* = 7.2 Hz), 7.66 (1H, s), 7.46 (1H, d, *J* = 8.0 Hz), 7.26 (1H, d, *J* = 7.6 Hz), 6.90 (1H, d, *J* = 4.0 Hz), 6.89 (1H, s), 6.78 (1H, d, *J* = 8.8 Hz), 6.72 (1H, dd, *J* = 2.4, 8.8 Hz), 3.86 (3H, s), 1.35 (12H, s). ^{13}C NMR ($(CD_3)_2O$, 100 MHz): δ 169.5, 162.6, 154.1, 153.2, 151.6, 136.3, 131.0, 130.4, 130.0, 128.3, 127.2, 125.7, 124.9, 123.8, 123.1, 112.8, 112.1, 106.7, 85.1, 82.7, 56.1, 25.5. HR-FABMS: calculated for [M^+] 457.1822, found 457.1831.

Fluorescein monotriflate (3)

Fluorescein (2.0 g, 5.8 mmol) and *N*-phenyl bis(trifluoromethanesulfonamide) (2.1 g, 5.8 mmol) were added to a dry schlenk flask and flushed with nitrogen. The reaction contents were dissolved in 15 mL of DMF and diisopropylethylamine (3.8 mL, 23.1 mmol) was added. After 48 hours of stirring the contents at room temperature, the reaction mixture was acidified with hydrochloric acid, extracted into ethyl acetate, and evaporated under reduced pressure. Purification by column chromatography (1:1 hexanes/ethyl acetate) afforded **3** as a pale yellow solid (1.7 g, 63%). ^{1}H NMR ($(CD_3)_2O$, 400 MHz): δ 8.01 (1H, d, *J* = 8.0 Hz), 7.81 (1H, dt, *J* = 1.2, 7.6 Hz), 7.75 (1H, dt, *J* = 1.2, 7.6 Hz), 7.50 (1H, d, *J* = 2.4 Hz). 7.36 (1H, d, *J* = 7.6 Hz), 7.21 (1H, dd, *J* = 2.4, 8.8 Hz), 7.09 (1H, d, *J* = 8.8 Hz), 6.81 (1H, d *J* = 2.4 Hz), 6.72 (1H, d, *J* = 8.8 Hz), 6.68 (1H, dd, *J* = 2.4, 8.8 Hz). ^{13}C NMR ($(CD_3)_2O$, 100 MHz): δ 168.2, 159.7, 152.6, 152.0, 151.8, 150.0, 135.5, 130.5, 130.3, 129.3, 126.3, 124.8, 124.0, 120.5, 117.0, 113.2, 110.4, 110.0, 102.5, 81.1. ^{19}F NMR ($(CD_3)_2O$, 376.5 MHz): δ-73.21. HR-FABMS: calculated for [M^+] 465.0256, found 465.0243.

Peroxyfluor-3, PF3 (4)

Compound **3** (200 mg, 0.43 mmol), Bis(pinacolato)diboron (111 mg, 0.43 mmol), Pd (dppf) Cl_2•CH_2Cl_2 (106 mg, 0.13 mmol), potassium acetate (127 mg, 1.29 mmol), and 10 mL of toluene were added to a dry pressure tube in an inert atmosphere glove box. The pressure tube was then brought out of the box and microwave-heated for 2 hours at 110 °C. After cooling the reaction mixture to room temperature, the contents of the pressure flask were washed into a round bottom flask with dichloromethane and evaporated to dryness. Purification by column chromatography (1:1 hexanes/ethyl acetate) delivered **4** as yellow solid (105 mg, 55%). ^{1}H NMR ($(CD_3)_2O$, 400 MHz): δ 8.00 (1H, d, *J* = 7.6 Hz), 7.76 (1H, t, *J* = 6.8 Hz), 7.70 (1H, t, *J* = 6.8 Hz), 7.64 (1H, s), 7.43 (1H, d, *J* = 7.6 Hz), 7.24 (1H, d, *J* = 7.6 Hz), 6.86 (1H, d, *J* = 8.0 Hz), 6.80 (1H, d, *J* = 2.0 Hz), 6.69 (1H, d, *J* = 8.4 Hz), 6.64 (1H, dd, *J* = 2.0, 8.4 Hz), 1.32 (12H, s). ^{13}C NMR ($(CD_3)_2O$, 100 MHz): δ 168.7, 159.7, 153.2, 152.2, 151.4, 150.7, 135.3, 130.0, 129.3, 129.1, 127.4, 126.3, 124.7, 123.9, 122.9, 122.2, 112.7, 110.1, 102.6, 84.1, 82.1, 24.3. HR-FABMS: calculated for [M^+] 443.1676, found 443.1666.

Peroxyfluor-3 acetate, PF3-Ac (5)

Compound **4** (33 mg, 0.08 mmol) and cesium carbonate (121 mg, 0.37 mmol) were added to a dry schlenk tube and dissolved in 3 mL of dry acetonitrile. Acetic anhydride (14 uL, 0.15 mmol) was added and the reaction stirred at room temperature for 30 minutes. The contents of the reaction were evaporated under reduced pressure. Purification by column chromatography (3:1 hexanes/ethyl acetate) afforded **5** as a clear film (16 mg, 43%). ^{1}H NMR ($CDCl_3$ /10% CD_3OD, 400 MHz): 8.04 (1H, d, *J* = 6.8 Hz), 7.75 (1H, s), 6.64 (2H, quintet, *J* = 7.2 Hz), 4.45 (1H, d, *J* = 7.6 Hz), 7.14 (1H, d, *J* = 7.2 Hz), 7.08 (1H, d, *J* = 2.0 Hz), 6.82 – 6.88 (2H, m), 6.80 (1H, dd, *J* = 2.0, 8.4 Hz), 2.32 (1H, s), 1.35 (12H, s). HR-FABMS: calculated for [M^+] 485.1772, found 485.1780.

Aniline rhodol triflate (6)

Rhodol (150 mg, 0.46 mmol) and *N*-phenyl bis(trifluoromethanesulfonamide) (250 mg, 0.69 mmol) were added to a glass vial and dissolved in 10 mL of acetonitrile. Diisopropylethylamine (0.23 mL, 1.4 mmol) was added and the reaction stirred at room temperature for 72 hours. The product was then extracted into ethyl acetate, washed once with water, and dried under reduced pressure. Purification by column chromatography (1:1 hexanes/ethyl acetate) yielded **6** as a white solid (49 mg, 23%). ^{1}H NMR ($(CD_3)_2O$, 400 MHz): δ 7.99 (1H, d, *J* = 7.6 Hz), 7.80 (1H, t, *J* = 7.6 Hz), 7.73 (1H, t, *J* = 7.2 Hz), 7.46 (1H, d, *J* = 2.0 Hz), 7.33 (1H, d, *J* = 7.6 Hz), 7.17 (1H, dd, *J* = 2.0, 8.8 Hz), 7.04 (1H, d, *J* = 8.8 Hz), 6.60 (1H, s), 6.52 (1H, d, *J* = 8.8 Hz), 6.48 (1H, d, *J* = 8.4 Hz). ^{13}C NMR ($(CD_3)_2O$, 100 MHz): δ 168.4, 152.6, 152.2, 152.0, 149.9, 135.4, 130.4, 130.1, 128.7, 126.7, 124.6, 124.0, 120.8, 118.7 (q, *J* = 318 Hz), 116.6, 112.0, 110.3, 106.1, 99.8, 81.9. ^{19}F NMR (Acetone, 376.5 MHz): δ-73.217. Low-res MS: 464.1.

Peroxy Emerald 1, PE1 (7)

6 (49 mg, 0.11 mmol), Bis(pinacolato)diboron (27 mg, 0.11 mmol), Pd (dppf) Cl_2•CH_2Cl_2 (26 mg, 0.03 mmol), and potassium acetate (31 mg, 0.32 mmol), and 3 mL of toluene were added to a dry pressure tube in an inert atmosphere glove box. The pressure tube was then brought out of the box and microwave-heated for 4 hours at 110 °C. After cooling to room temperature, the reaction contents were washed into a round bottom flask with dichloromethane and methanol and dried under reduced pressure. Purification by column chromatography (1:1 hexanes/ethyl acetate) yielded PE1 as a light orange solid (7 mg, 15%). ^{1}H NMR (Acetone, 400 MHz): δ 7.99 (1H, d, *J* = 7.6 Hz), 7.78 (1H, t, *J* = 7.6 Hz), 7.72 (1H, t, *J* = 7.6 Hz), 7.62 (1H, s), 7.41 (1H, d, *J* = 7.6 Hz), 7.26 (1H, d, *J* = 7.6 Hz), 6.83 (1H, d, *J* = 7.6 Hz), 6.60 (1H, d, *J* = 2.0 Hz), 6.52 (1H, d, *J* = 8.8 Hz), 6.45 (1H, dd, *J* = 2.0, 8.8 Hz), 1.34 (12H, s). ^{13}C NMR (Acetone, 100 MHz): δ 169.6, 154.2, 153.3, 152.1, 151.9, 136.1, 130.8, 129.9, 129.6, 128.3,

127.7, 125.4, 124.9, 123.8, 123.4, 112.4, 107.4, 100.9, 85.0, 83.7, 74.9, 25.2. HR-FABMS: calculated for [M^+] 442.1831, found 442.1820.

Diethylamino rhodol (8)

Synthesis adopted from literature.[101] 2-(4-Diethylamino-2-hydroxybenzoyl)benzoic acid (1.26 g, 4.0 mmol) and resorcinol (443 g, 4.0 mmol) were added to a heavy-walled pressure flask and dissolved in 15 mL of trifluoroacetic acid. The reaction contents were heated to 90 °C for 12 hours, then cooled to room temperature and evaporated to dryness. Purification by column chromatography (4.5:4.5:1 dichloromethane/ethyl acetate/methanol) delivered **8** as a red-brown solid (1.2 g, 77% yield). ^{1}H NMR ($CDCl_3$ /10% CD_3OD, 400 MHz): δ 8.19 (1H, d, *J* = 7.2 Hz), 7.59 (2H, quartet, *J* = 7.2 Hz), 7.11 (1H, d, *J*=7.2 Hz), 6.86–6.95 (3H, m), 6.68 (2H, dd, *J* = 2.0, 9.2 Hz), 6.64 (1H, d, *J* = 2.0 Hz), 3.44 (4H, q, *J* = 7.2 Hz), 1.16 (6H, t, *J* = 7.2 Hz). ^{13}C NMR ($CDCl_3$ /10% CD_3OD, 100 MHz): δ 163.5, 153.4, 152.4, 150.9, 128.9, 127.3, 126.7, 126.2, 126.0, 124.4, 113.2, 110.0, 109.7, 108.7, 98.6, 92.3, 41.8, 8.3. HR-FABMS: calculated for [M^+] 388.1549, found 388.1546.

Diethylamino rhodol triflate (9)

Compound **8** (500 mg, 1.39 mmol) and *N*-phenyl bis(trifluoromethanesulfonamide) (745 mg, 2.09 mmol) were added to a vial and flushed with nitrogen. The reaction contents were dissolved in 5 mL of DMF, and diisopropylethylamine (691 uL, 4.18 mmol) was added. After 10 min of stirring at room temperature, the product was extracted into ethyl acetate, washed three times with water, and evaporated under reduced pressure. Purification by column chromatography (3:1 hexanes/ethyl acetate) afforded **9** as a light pink solid (440 mg, 61%). ^{1}H NMR ($CDCl_3$ /10% CD_3OD, 400 MHz): δ 7.99 (1H, d, *J* = 7.6 Hz), 7.65 (1H, t, *J* = 7.2 Hz), 7.60 (1H, t, *J* = 7.2 Hz), 7.20 (1H, d, *J* = 2.4 Hz), 7.17 (1H, d, *J* = 7.6 Hz), 6.90 (1H, dd, *J* = 2.4, 8.8 Hz), 6.84 (1H, d, *J* = 8.8 Hz), 6.54 (1H, d, *J* = 9.2 Hz), 6.44 (1H, d, *J* = 2.4 Hz), 6.36 (1H, dd, *J* = 2.4, 8.8 Hz), 3.31 (4 H, q, *J* = 7.2 Hz), 1.11 (6H, t, *J* = 7.2 Hz). ^{13}C NMR ($CDCl_3$ /10% CD_3OD, 100 MHz): δ 169.5, 152.5, 152.4, 152.4, 149.8, 149.8, 135.3, 130.0, 129.2, 128.7, 126.7, 125.0, 124.0, 123.4, 120.2, 116.1, 113.8, 110.3, 109.0, 104.1, 97.4, 83.1, 44.4, 12.3. ^{19}F NMR ($CDCl_3$ /10% CD_3OD, 376.5 MHz): δ-72.05. HR-FABMS: calculated for [M^+] 520.1042, found 520.1036.

Peroxy Yellow 1, PY1 (10)

Compound **9** (200 mg, 0.38 mmol), Bis(pinacolato)diboron (94 mg, 0.38 mmol), Pd (dppf) Cl_2•CH_2Cl_2 (94 mg, 0.12 mmol), potassium acetate (113 mg, 1.16 mmol), and 3 mL of toluene were added to a dry pressure tube in an inert atmosphere glove box. The pressure tube was then brought out of the box and microwave-heated for 2 hours at 110 °C. After cooling the reaction mixture to room temperature, the contents of the pressure flask were washed into a round bottom flask with dichloromethane and evaporated to dryness. Purification by column chromatography (4:1 hexanes/ethyl acetate) delivered PY1 as light tan solid (41 mg, 22%). ^{1}H NMR ($CDCl_3$ /10% CD_3OD, 400 MHz): δ 7.98 (1H, d, *J* = 7.6 Hz), 7.69 (1H, s), 7.62 (1H, t, *J* = 7.2 Hz), 7.58 (1H, t, *J* = 7.2 Hz), 7.35 (1H, d, *J* = 7.6 Hz), 7.13 (1H, d, *J* = 7.2 Hz), 6.73 (1H, d, *J* = 8.0 Hz), 6.55 (1H, d, *J* = 9.2 Hz), 6.433 (1H, s), 6.34 (1H, d, *J* = 8.8 Hz) 3.33 (4H, q, *J* = 7.2 Hz), 1.31 (12H, s), 1.14 (6H, t, *J* = 7.2Hz). ^{13}C NMR ($CDCl_3$ /10% CD_3OD, 100 MHz): δ 170.1, 153.2, 152.8, 151.1, 134.9, 129.6, 128.8, 128.8, 127.2, 126.7, 124.9, 124.0, 123.9, 121.8, 84.2, 44.5, 12.4. HR-FABMS: calculated for [M^+] 498.2452, found 498.2441.

Julolidine rhodol (11)

Synthesis adopted from literature.[101] 8-Hydroxy-9-o-carboxybenzoyljulolidine (3.23 g, 9.56 mmol) and resorcinol (1.05 g, 9.56 mmol) were added to a heavy-walled pressure flask and

dissolved in 20 mL of methane sulfonic acid. The reaction contents were heated to 90 °C for 3 hours, then cooled to room temperature and basified with aqueous sodium hydroxide. The mixture was then extrated into ethyl acetate and evaporated under reduced pressure. Purification by column chromatography (4.5:4.5:2 dichloromethane/ethyl acetate/methanol) delivered **11** as a maroon solid (2.5g, 63% yield). ^{1}H NMR ($CDCl_3$ /10% CD_3OD, 400 MHz): δ 8.01 (1H, d, *J* = 7.2 Hz), 7.46 (2H, quartet, *J* = 8.8 Hz), 7.02 (1H, d, *J* = 7.2 Hz), 6.92 (1H, d, *J* = 9.2 Hz), 6.64 (1H, s), 6.58 (1H, s), 6.49 (1H, d, *J* = 7.6 Hz), 3.33 (4H, quintet, *J* = 6.0 Hz), 2.86 (2H, d, *J* = 6.4 Hz), 2.50 – 2.58 (2H, m), 1.72 – 1.99 (4H, m). ^{13}C NMR ($CDCl_3$ / 10% CD_3OD, 100 MHz): δ 174.6, 167.8, 153.9, 148.1, 146.4, 134.0, 126.9, 125.9, 125.8, 125.3, 125.0, 122.9, 118.5, 117.4, 109.7, 108.7, 100.9, 99.0, 46.7, 46.2, 23.4, 16.7, 15.8. HR-FABMS: calculated for [M^+] 412.1549, found 412.1555.

Julolidine rhodol triflate (12)

Compound **11** (500 mg, 1.2 mmol) and *N*-phenyl bis(trifluoromethanesulfonamide) (868 mg, 2.4 mmol) were added to a vial and flushed with nitrogen. The reaction contents were dissolved in 5 mL of DMF, and diisopropylethylamine (805 uL, 4.9 mmol) was added. After 20 min of stirring at room temperature, the product was extracted into ethyl acetate, washed three times with water, and evaporated under reduced pressure. Purification by column chromatography (1:1 hexanes/ethyl acetate) afforded **12** as a light red solid (224 mg, 34%). ^{1}H NMR ($(CD_3)_2O$, 400 MHz): δ 7.98 (1H, d, *J* = 7.6 Hz), 7.79 (1H, t, *J* = 7.2 Hz), 7.73 (1H, t, *J* = 7.6 Hz), 7.52 (1H, d, *J* = 2.8 Hz), 7.31 (1H, d, *J* =7.6 Hz), 7.15 (1H dd, *J* = 2.4, 8.8 Hz), 7.00 (1H, d, *J* = 8.8 Hz), 6.19 (1H, s), 3.20 (2H, t, *J* = 6.0 Hz), 3.15 (2H, t, *J* = 6.0 Hz), 2.91 (2H, t, *J* = 6.8 Hz), 2.41–2.59 (2H, m), 1.92–2.00 (2H, m), 1.76–1.86 (2H, m). ^{13}C NMR ($(CD_3)_2O$ /10% CD_3OD, 100 MHz): δ 168.3, 152.5, 152.4, 149.9, 147.3, 144.7, 135.2, 130.3, 130.0, 126.9, 124.6, 124.5, 124.1, 120.7, 118.5, 116.3, 110.4, 106.8, 104.5, 82.6, 49.4, 48.9, 21.4, 20.8, 20.7, 19.9. ^{19}F NMR ($(CD_3)_2O$, 376.5 MHz): δ-73.284. HR-FABMS: calculated for [M^+] 544.1042, found 544.1036.

Peroxy Orange 1, PO1 (13)

Compound **1 2** (100 mg, 0.18 mmol), Bis(pinacolato)diboron (47 mg, 0.18 mmol), Pd (dppf) Cl_2•CH_2Cl_2 (45 mg, 0.05 mmol), potassium acetate (55 mg, 0.55 mmol), and 5 mL of toluene were added to a dry pressure tube in an inert atmosphere glove box. The pressure tube was then brought out of the box and microwave-heated for 2 hours at 110 °C. After cooling the reaction mixture to room temperature, the contents of the pressure flask were washed into a round bottom flask with dichloromethane and evaporated to dryness. Purification by column chromatography (4.5:4.5:1 dichloromethane/ethyl acetate/methanol) delivered PO1 as light red solid (36 mg, 38%). ^{1}H NMR ($CDCl_3$ /10% CD_3OD, 400 MHz): δ 7.95 (1H, d, *J* = 7.2 Hz), 7.40 (1H, s), 7.58 (1H, t, *J* = 7.2 Hz), 7.54 (1H, t, *J* = 7.2 Hz), 7.33 (1H, d, *J* = 8.0 Hz), 7.11 (1H, d, *J* = 7.6 Hz), 6.69 (1H, d, *J* = 7.6 Hz), 6.10 (1H, s), 3.10 (2H, t, *J* = 5.2 Hz), 3.06 (2H, t, *J* = 5.2 Hz), 2.87 (2H, t, *J* = 6.4 Hz), 2.37–2.54 (2H, m), 1.91–1.99 (2H, m), 1.79 (2H, t, *J* = 5.2 Hz), 1.28 (12H, s). ^{13}C NMR ($CDCl_3$/10% CD_3OD, 100 MHz): δ 170.1, 153.2, 151.1, 147.8, 144.7, 134.9, 129.5, 128.6, 127.1, 126.8, 124.8, 124.6, 124.0, 123.5, 121.6, 117.8, 107.2, 104.5, 85.1, 84.1, 74.9, 49.7, 49.3, 27.3, 24.8, 21.6, 21.1, 20.9. HR-FABMS: calculated for [M^+] 522.2456, found 522.2452.

Spectroscopic Materials and Methods

Millipore water was used to prepare all aqueous solutions. All spectroscopic measurements were performed in 20 mM HEPES buffer, pH 7. Absorption spectra were recorded on a Varian Cary 50 spectrophotometer (Walnut Creek, CA) and fluorescence spectra were recorded on a Photon Technology International Quanta Master 4 L-format scanning spectrofluorometer (Lawrenceville, NJ) equipped with an LPS-220B 75-W xenon lamp and power supply,

A-1010B lamp housing with integrated igniter, switchable 814 photon-counting/analog photomultiplier detection unit, and MD5020 motor driver. Samples for absorption and emission measurements were contained in 1-cm × 1-cm quartz cuvettes (1.5-mL volume, Starna, Atascadero, CA). Fluorescence quantum yields were determined by reference to fluorescein in 0.1M NaOH ($\Phi = 0.94$) or rhodamine B in water ($\Phi = 0.31$).

Preparation and Staining of Cell Cultures

RAW264.7 macrophages were cultured in Dulbecco's Modified Eagle Medium (DMEM) containing high glucose with GlutaMAX™ (Invitrogen, Carlsbad, CA) and supplemented with 10% Fetal Bovine Serum (FBS, Hyclone). A431 cells were cultured in DMEM plus GlutaMAX™ supplemented with 10% FBS. Cells were split 1/30 twice a week. Two days before imaging, cells were passed and plated on 18- mm glass coverslips coated with poly-L-lysine (50 μg/mL, Sigma, St. Louis, MO). 18 hours before imaging, A431 cells that were to be used for EGF stimulation experiments were serum-starved in DMEM alone. For all experiments, solutions of dyes (from 5 mM stocks in DMSO) were made in DPBS with calcium chloride and magnesium chloride (Sigma). H_2O_2 (100 mM stock solution in Millipore water), HOCl (100 mM stock solution in Millipore water), phorbol myristate acetate (PMA, 1 mg/mL stock solution in DMSO), or EGF (100 μg/mL stock in Millipore water) were added by bath application to the cell culture media. The cells were then kept in an incubator (37 °C, 5% CO_2) during the course of all experiments.

Fluorescence Imaging Experiments

Confocal fluorescence imaging studies were performed with a Zeiss LSM510 NLO Axiovert 200 laser scanning microscope and a 40× or 63× Achroplan IR water-immersion objective lens. Excitation of PF2 and PF3-loaded cells at 488 nm was carried out with an Ar laser and emission was collected using a META detector between 495–581 nm. Excitation of PY1-loaded cells at 514 nm was carried out with an Ar laser and emission was collected using a META detector between 516–581 nm. Excitation of PO1-loaded cells at 543 nm was carried out with an HeNe laser and emission was collected using a META detector between 548–613 nm. Excitation of Hoechst 33342 was carried out using a MaiTai two-photon laser at 780-nm pulses (mode-locked Ti:sapphire laser, Tsunami Spectra Physics) and emission was collected between 452–537 nm. Excitation of PO1 and APF-loaded cells at 488 and 543 nm was carried out with Ar and HeNe lasers, respectively, and emission was collected using a META detector between 495–538 and 548–602 nm, respectively, using sequential scans. Image analysis was performed in Image J.

Supplementary Material

Refer to Web version on PubMed Central for supplementary material.

Acknowledgments

We thank the Packard and Sloan Foundations, the Hellman Faculty Fund (UC Berkeley), Amgen, Astra Zeneca, Novartis, and the National Institute of General Medical Sciences (NIH GM 79465) for funding this work. C.J.C. is an Investigator with the Howard Hughes Medical Institute. B.C.D. thanks the NIH Chemical Biology Graduate Program (T32 GM066698) for support, and C.H. thanks the Department of Chemistry at UC Berkeley for a Summer Undergraduate Research award. We thank Holly Aaron (UCB Molecular Imaging Center) and Ann Fischer (UCB Tissue Culture Facility) for expert technical assistance and helpful discussions.

References

1. Harman D. Proc. Natl. Acad. Sci. USA 1981;78:7124–7128. [PubMed: 6947277]
2. Floyd RA. Science 1991;254:1597. [PubMed: 1684251]

3. Giorgio M, Trinei M, Migliaccio E, Pelicci PG. Nat. Rev. Mol. Cell. Biol 2007;8:722–728. [PubMed: 17700625]
4. Zhang W, Wang T, Qin L, Gao HM, Wilson B, Ali SF, Hong JS, Liu B. FASEB J 2004;18:589–591. [PubMed: 14734632]
5. Finkel T, Serrano M, Blasco MA. Nature 2007;448:767–774. [PubMed: 17700693]
6. Park L, Zhou P, Pitstick R, Capone C, Anrather J, Norris EH, Younkin L, Younkin S, Carlson G, McEwen BS, Iadecola C. Proc. Natl. Acad. Sci. USA 2008;105:1347–1352. [PubMed: 18202172]
7. Andersen JK. Nat. Rev. Neurosci 2004:S18–S25.
8. Barnham KJ, Masters CL, Bush AI. Nat. Rev. Drug Discovery 2004;3:205–214.
9. Sundaresan M, Yu ZX, Ferrans VJ, Irani K, Finkel T. Science 1995;270:296–299. [PubMed: 7569979]
10. Bae YS, Kang SW, Seo MS, Baines IC, Tekle E, Chock PB, Rhee SG. J. Biol. Chem 1997;272:217–221. [PubMed: 8995250]
11. Avshalumov MV, Rice ME. Proc. Natl Acad. Sci. USA 2003;100:11729–11734. [PubMed: 13679582]
12. Lambeth JD. Nat. Rev. Immunol 2004;4:181–189. [PubMed: 15039755]
13. Rhee SG. Science 2006;312:1882–1883. [PubMed: 16809515]
14. Stone JR, Yang S. Antioxid. Redox Signal 2006;8:243–270. [PubMed: 16677071]
15. Miller EW, Chang CJ. Curr. Opin. Chem. Biol 2007;11:620–625. [PubMed: 17967434]
16. Miller EW, Tulyathan O, Isacoff EY, Chang CJ. Nat. Chem. Biol 2007;3:263–267. [PubMed: 17401379]
17. Veal EA, Day AM, Morgan BA. Mol. Cell 2007;26:1–14. [PubMed: 17434122]
18. Winterbourn CC. Nat. Chem. Biol 2008;4:278–286. [PubMed: 18421291]
19. Poole LB, Nelson KJ. Curr. Opin. Chem. Biol 2008;12:18–24. [PubMed: 18282483]
20. Paulsen CE, Carroll KS. ACS Chem. Biol 2010;5:47–62. [PubMed: 19957967]
21. Murphy MP. Biochem. J 2009;417:1–13. [PubMed: 19061483]
22. Dickinson BC, Srikun D, Chang CJ. Curr. Opin. Chem. Biol 2010;14:50–56. [PubMed: 19910238]
23. Shaner NC, Steinbach PA, Tsien RY. Nat. Meth 2005;2:905–909.
24. Giepmans BNG, Adams SR, Ellisman MH, Tsien RY. Science 2006;312:217–224. [PubMed: 16614209]
25. Soh N. Anal. Bioanal. Chem 2006;386:532–543. [PubMed: 16609844]
26. Domaille DW, Que EL, Chang CJ. Nat. Chem. Biol 2008;4:168–175. [PubMed: 18277978]
27. Terai T, Nagano T. Curr. Opin. Chem. Biol 2008;12:515–521. [PubMed: 18771748]
28. Lavis LD, Raines RT. ACS Chem. Biol 2008;3:142–155. [PubMed: 18355003]
29. Laughlin ST, Bertozzi CR. Proc. Natl. Acad. Sci. USA 2009;106:12–17. [PubMed: 19104067]
30. Kojima H, Nakatsubo N, Kikuchi K, Kawahara S, Kirino Y, Nagoshi H, Hirata Y, Nagano T. Anal. Chem 1998;70:2446–2453. [PubMed: 9666719]
31. Kojima H, Hirotani M, Nakatsubo N, Kikuchi K, Urano Y, Higuchi T, Hirata Y, Nagano T. Anal. Chem 2001;73:1967–1973. [PubMed: 11354477]
32. Gabe Y, Urano Y, Kikuchi K, Kojima H, Nagano T. J. Am. Chem. Soc 2004;126:3357–3367. [PubMed: 15012166]
33. Sasaki E, Kojima H, Nishimatsu H, Urano Y, Kikuchi K, Hirata Y, Nagano T. J. Am. Chem. Soc 2005;127:3684–3685. [PubMed: 15771488]
34. Lim MH, Xu D, Lippard SJ. Nat. Chem. Biol 2006;2:375–380. [PubMed: 16732295]
35. Lim MH, Lippard SJ. Acc. Chem. Res 2007;40:41–51. [PubMed: 17226944]
36. McQuade LE, Lippard SJ. Curr. Opin. Chem. Biol 2010;14:43–49. [PubMed: 19926519]
37. Yang D, Wang HL, Sun ZN, Chung NW, Shen JG. J. Am. Chem. Soc 2006;128:6004–6005. [PubMed: 16669647]
38. Sun ZN, Wang HL, Liu FQ, Chen Y, Tam PKH, Yang D. Org. Lett 2009;11:1887–1890. [PubMed: 19331349]
39. Ueno T, Urano Y, Kojima H, Nagano T. J. Am. Chem. Soc 2006;128:10640–10641. [PubMed: 16910633]

40. Maeda H, Yamamoto K, Nomura Y, Kohno I, Hafsi L, Ueda N, Yoshida S, Fukuda M, Fukuyasu Y, Yamauchi Y. J. Am. Chem. Soc 2005;127:68–69. [PubMed: 15631452]
41. Robinson KM, Janes MS, Pehar M, Monette JS, Ross MF, Hagen TM, Murphy MP, Beckman JS. Proc. Natl Acad. Sci. USA 2006;103:15038–15043. [PubMed: 17015830]
42. Xu K, Liu X, Tang B, Yang G, Yang Y, An L. Chem. Eur. J 2007;13:1411–1416.
43. Xu K, Liu X, Tang B. ChemBioChem 2007;8:453–458. [PubMed: 17238211]
44. Umezawa N, Tanaka K, Urano Y, Kikuchi K, Higuchi T, Nagano T. Angew. Chem. Int. Ed 1999;38:2899–2901.
45. Song B, Wang G, Tan M, Yuan J. J. Am. Chem. Soc 2006;128:13442–13450. [PubMed: 17031957]
46. Garner AL, St Croix CM, Pitt BR, Leikauf GD, Ando S, Koide K. Nat. Chem 2009;1:316–321.
47. Wolfbeis OS, Dürkop A, Wu M, Lin Z. Angew. Chem. Int. Ed 2002;41:4495–4498.
48. Meng O, Lin WZ. Angew. Chem. Int. Ed 2002;41:4495–4498.
49. Onoda M, Uchiyama S, Endo A, Tokuyama H, Santa T, Imai K. Org. Lett 2003;5:1459–1461. [PubMed: 12713298]
50. Lo LC, Chu CY. Chem. Commun 2003:2728–2729.
51. Chang MCY, Pralle A, Isacoff EY, Chang CJ. J. Am. Chem. Soc 2004;126:15392–15393. [PubMed: 15563161]
52. Maeda H, Fukuyasu Y, Yoshida S, Fukuda M, Saeki K, Matsuno H, Yamauchi Y, Yoshida K, Hirata K, Miyamoto K. Angew. Chem. Int. Ed 2004;43:2389–2391.
53. Miller EW, Albers AE, Pralle A, Isacoff EY, Chang CJ. J. Am. Chem. Soc 2005;127:16652–16659. [PubMed: 16305254]
54. Kozhevnikov VN, Mandl C, Miltschitzky S, Duerkop A, Wolfbeis OS, Koenig B. Inorg. Chim. Acta 2005;358:2445–2448.
55. Soh N, Sakawaki O, Makihara K, Odo Y, Fukaminato T, Kawai T, Irie M, Imato T. Bioorg. Med. Chem. Lett 2005;13:1131–1139.
56. Onoda M, Tokuyama H, Uchiyama S, Mawatari K, Santa T, Kaneko K, Imai K, Nakagomi K. Chem. Commun 2005;2005:1848–1850.
57. Belousov VV, Fradkov AF, Lukyanov KA, Staroverov DB, Shakhbazov KS, Terskikh AV, Lukyanov S. Nat. Methods 2006;3:281–286. [PubMed: 16554833]
58. Albers AE, Okreglak VS, Chang CJ. J. Am. Chem. Soc 2006;128:9640–9641. [PubMed: 16866512]
59. Lee D, Khaja S, Velasquez-Castano JC, Dasari M, Sun C, Petros J, Taylor WR, Murthy N. Nat. Mater 2007;6:765–769. [PubMed: 17704780]
60. Srikun D, Miller EW, Domaille DW, Chang CJ. J. Am. Chem. Soc 2008;130:4596–4597. [PubMed: 18336027]
61. Dickinson BC, Chang CJ. J. Am. Chem. Soc 2008;130:9638–9639. [PubMed: 18605728]
62. Albers AE, Dickinson BC, Miller EW, Chang CJ. Bioorg. Med. Chem. Lett 2008;18:5948–5950. [PubMed: 18762422]
63. Xu K, Liu F, Wang H, Wang S, Wang L, Tang B. Sci. China, Ser. B Chem 2009;52:734–740.
64. Du YL, Ni YN, Li M, Wang B. Tetrahedron Letters 2010;51:1152–1154. [PubMed: 20204162]
65. Srikun D, Albers AE, Nam CI, Ivarone AT, Chang CJ. J. Am. Chem. Soc 2010;132 ASAP.
66. Kenmoku S, Urano Y, Kojima H, Nagano T. J. Am. Chem. Soc 2007;129:7313–7318. [PubMed: 17506554]
67. Sun ZN, Liu FQ, Chen Y, Tam PKH, Yang D. Org. Lett 2008;10:2171–2174. [PubMed: 18447382]
68. Setsukinai K, Urano Y, Kakinuma K, Majima HJ, Nagano T. J. Biol. Chem 2003;278:3170–3175. [PubMed: 12419811]
69. Koide Y, Urano Y, Kenmoku S, Kojima H, Nagano T. J. Am. Chem. Soc 2007;129:10324–10325. [PubMed: 17672465]
70. Panizzi P, Nahrendorf M, Wildgruber M, Waterman P, Figueiredo JL, Aikawa E, McCarthy J, Weissleder R, Hilderbrand SA. J. Am. Chem. Soc 2009;131:15739–15744. [PubMed: 19817443]
71. Hempel SL, Buettner GR, O'Malley YQ, Wessels DA, Flaherty DM. Free Radical Biol. Med 1999;27:146–159. [PubMed: 10443931]

72. Østergaard H, Henriksen A, Hansen FG, Winther JR. EMBO J 2001;20:5853–5863. [PubMed: 11689426]
73. Hanson GT, Aggeler R, Oglesbee D, Cannon M, Capaldi RA, Tsien RY, Remington SJ. J. Biol. Chem 2004;279:13044–13053. [PubMed: 14722062]
74. Cline DJ, Thorpe C, Schneider JP. Anal. Biochem 2004;325:144–150. [PubMed: 14715295]
75. Lee K, Dzubeck V, Latshaw L, Schneider JP. J. Am. Chem. Soc 2004;126:13616–13617. [PubMed: 15493909]
76. Cannon MB, Remington SJ. Protein Sci 2006;15:45–57. [PubMed: 16322566]
77. Miller EW, Bian SX, Chang CJ. J. Am. Chem. Soc 2007;129:3458–3459. [PubMed: 17335279]
78. Ahn YH, Lee JS, Chang YT. J. Am. Chem. Soc 2007;129:4510–4511. [PubMed: 17378562]
79. Wang W, Fang H, Groom L, Cheng A, Zhang W, Liu J, Wang X, Li K, Han P, Zheng M. Cell 2008;134:279–290. [PubMed: 18662543]
80. Gutscher M, Pauleau AL, Marty L, Brach T, Wabnitz GH, Samstag Y, Meyer AJ, Dick TP. Nat. Methods 2008;5:553–560. [PubMed: 18469822]
81. Banerjee S, Kar S, Perez JM, Santra S. J. Phys. Chem. C 2009;113:9659–9663.
82. Shao N, Jin J, Wang H, Zheng J, Yang R, Chan W, Abliz Z. J. Am. Chem. Soc 2009;132:725–736. [PubMed: 20030359]
83. Kundu K, Knight SF, Willett N, Lee S, Taylor WR, Murthy N. Angew. Chem. Int. Ed 2009;48:299–303.
84. Oushiki D, Kojima H, Terai T, Arita M, Hanaoka K, Urano Y, Nagano T. J. Am. Chem. Soc 2010;132 ASAP.
85. Burdette SC, Lippard SJ. Inorg. Chem 2002;41:6816–6823. [PubMed: 12470079]
86. Clark MA, Duffy K, Tibrewala J, Lippard SJ. Org. Lett 2003;5:2051–2054. [PubMed: 12790526]
87. Woodroofe CC, Lim MH, Bu W, Lippard SJ. Tetrahedron 2005;61:3097–3105.
88. Hilderbrand SA, Weissleder R. Tettrahedron Lett 2007;48:4383–4385.
89. Wu L, Burgess K. Org. Lett 2008;10:1779–1782. [PubMed: 18396890]
90. Li J, Yao SQ. Org. Lett 2008;11:405–408. [PubMed: 19099491]
91. Li J, Hu M, Yao SQ. Org. Lett 2009;11:3008–3011. [PubMed: 19522535]
92. Peng T, Yang D. Org. Lett 2010;12:496–499. [PubMed: 20067265]
93. Wrona M, Patel K, Wardman P. Free Radical Biology and Medicine 2005;38:262–270. [PubMed: 15607909]
94. Li H, Li Q, Wang X, Xu K, Chen Z, Gong X, Liu X, Tong L, Tang B. Analytical Chemistry 2009;81:2193–2198.
95. Gong X, Li Q, Xu K, Liu X, Li H, Chen Z, Tong L, Tang B, Zhong H. Electrophoresis 2009;30:1983–1990. [PubMed: 19517439]
96. Hampton MB, Kettle AJ, Winterbourn CC. Blood 1998;92:3007–3017. [PubMed: 9787133]
97. Winterbourn CC, Vissers M, Kettle AJ. Curr. Opin. Hematol 2000;7:53–58. [PubMed: 10608505]
98. Karlsson A, Dahlgren C. Antioxid. Redox Signal 2002;4:49–60. [PubMed: 11970843]
99. van der Veen BS, de Winther MPJ, Heeringa P, Augusto O, Chen JW, Davies M, Ma XL, Malle E, Pignatelli P, Rudolph T. Antioxid. Redox Signal 2009;11:2899–2937. [PubMed: 19622015]
100. Patel SV, Patel MP, Patel RG. J. Serb. Chem. Soc 2005;70:931–936.
101. Sauers RR, Husain SN, Piechowski AP, Bird GR. Dyes Pigm 1987;8:35–53.
102. Whitaker JE, Haugland RP, Ryan D, Hewitt PC, Haugland RP, Prendergast FG. Anal. Biochem 1992;207:267–279. [PubMed: 1481981]
103. Mugherli L, Burchak ON, Chatelain F, Balakirev MY. Bioorg. Med. Chem. Lett 2006;16:4488–4491. [PubMed: 16806926]
104. Heller CA, Henry RA, McLaughlin BA, Bliss DE. J. Chem. Eng. Data 1974;19:214–219.

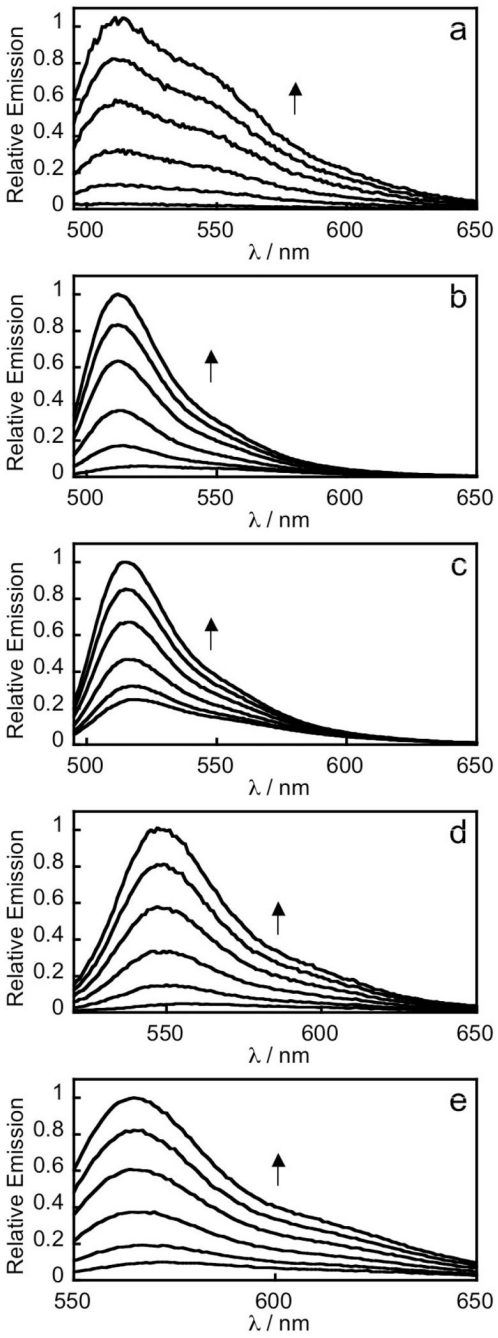

Figure 1.

Fluorescence turn-on response of 5 μM PF2 (a), PF3 (b), PE1 (c), PY1 (d) or PO1 (e) to H_2O_2. Data were acquired at 25 °C in 20 mM HEPES, pH 7, with excitation at λ = 488 nm for PF2 and PF3, λ = 490 nm for PE1, λ = 514 nm for PY1, and λ = 540 nm for PO1. Emission was collected between 493 and 750 nm for PF2 and PF3, 495 and 750 nm for PE1, 520 and 750 nm for PY1 and 545 and 750 nm for PO1. Time points represent 0, 5, 15, 30, 45, and 60 minutes after the addition of 100 μM H_2O_2. Reactions are not complete at these time points. Full turn-on response of each probe is shown in Fig. S1.

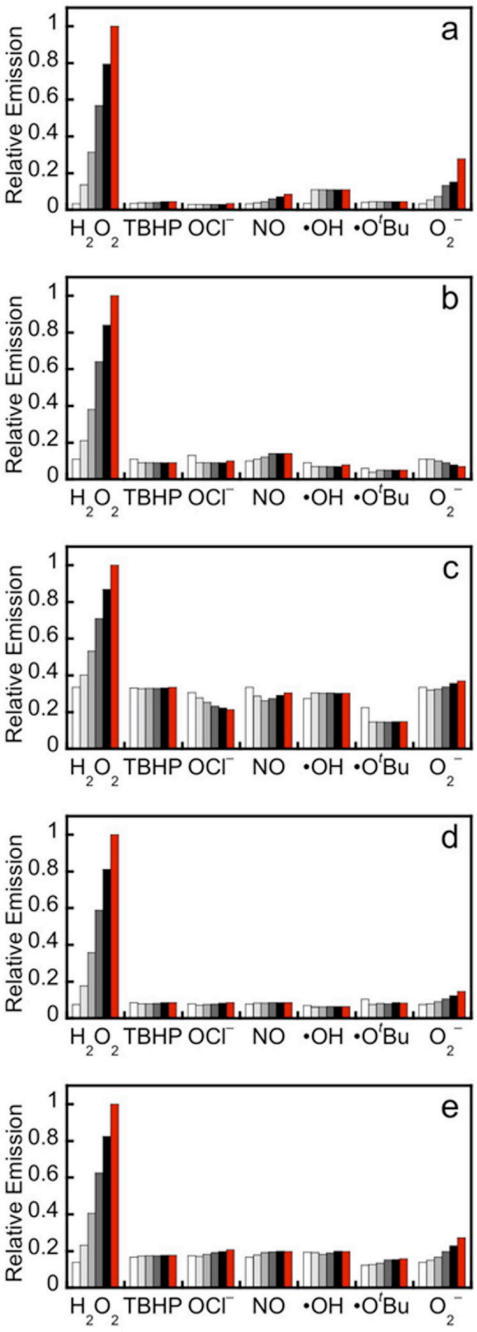

Figure 2.

Fluorescence responses of 5 μM PF2 (a), PF3 (b), PE1 (c), PY1 (d) and PO1 (e) to various reactive oxygen species (ROS). Bars represent relative responses at 0, 5, 15, 30, 45, and 60 min after addition of each ROS. Data shown are for 200 μM NO and 100 μM for all other ROS. Data were acquired at 25 °C in 20 mM HEPES, pH 7, with excitation at λ = 488 nm for PF2 and PF3, λ = 490 nm for PE1, λ = 514 nm for PY1, and λ = 540 nm for PO1. Emission was collected between 493 and 750 nm for PF2 and PF3, 495 and 750 nm for PE1, 520 and 750 nm for PY1 and 545 and 750 nm for PO1. Time points represent 0, 5, 15, 30, 45, and 60 minutes after the addition of 100 μM H_2O_2. Reactions are not complete at these time points.

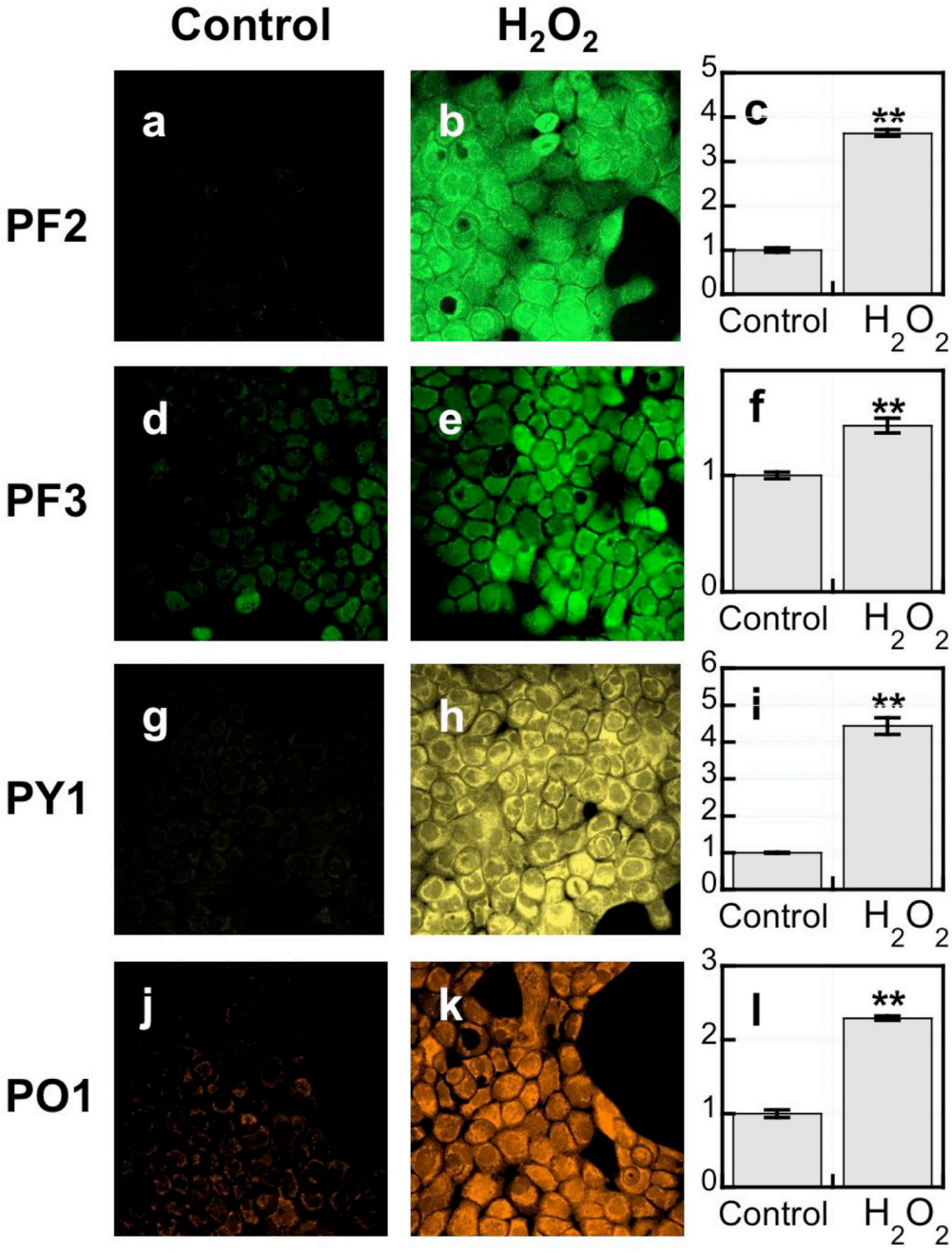

Figure 3.

Confocal fluorescence images of H_2O_2 in live A431 cells under oxidative stress with PF2, PF3-Ac, PY1 and PO1. A431 cells incubated with 10 μM PF2 for 40 min at 37 °C (a). A431 cells incubated with 10 μM PF2 for 40 min at 37 °C with 100 μM H_2O_2 added for the final 20 min (b) and quantification (c). A431 cells incubated with 5 μM PF3-Ac for 40 min at 37 °C (d). A431 cells incubated with 5 μM PF3-Ac for 40 min at 37 °C with 100 μM H_2O_2 added for the final 20 min (e) and quantification (f). A431 cells incubated with 5 μM PY1 for 40 min at 37 °C (g). A431 cells incubated with 5 μM PY1 for 40 min at 37 °C with 100 μM H_2O_2 added for the final 20 min (h) and quantification (i). A431 cells incubated with 5 μM PO1 for 40 min at 37 °C (j). A431 cells incubated with 5 μM PO1 for 40 min at 37 °C with 100 μM H_2O_2

added for the final 20 min (k) and quantification (l). Data were normalized to controls and statistical analyses were performed with a two-tailed Student's *t*-test (n = 4). $^{**}P \leq 0.005$ and error bars are ± s.e.m.

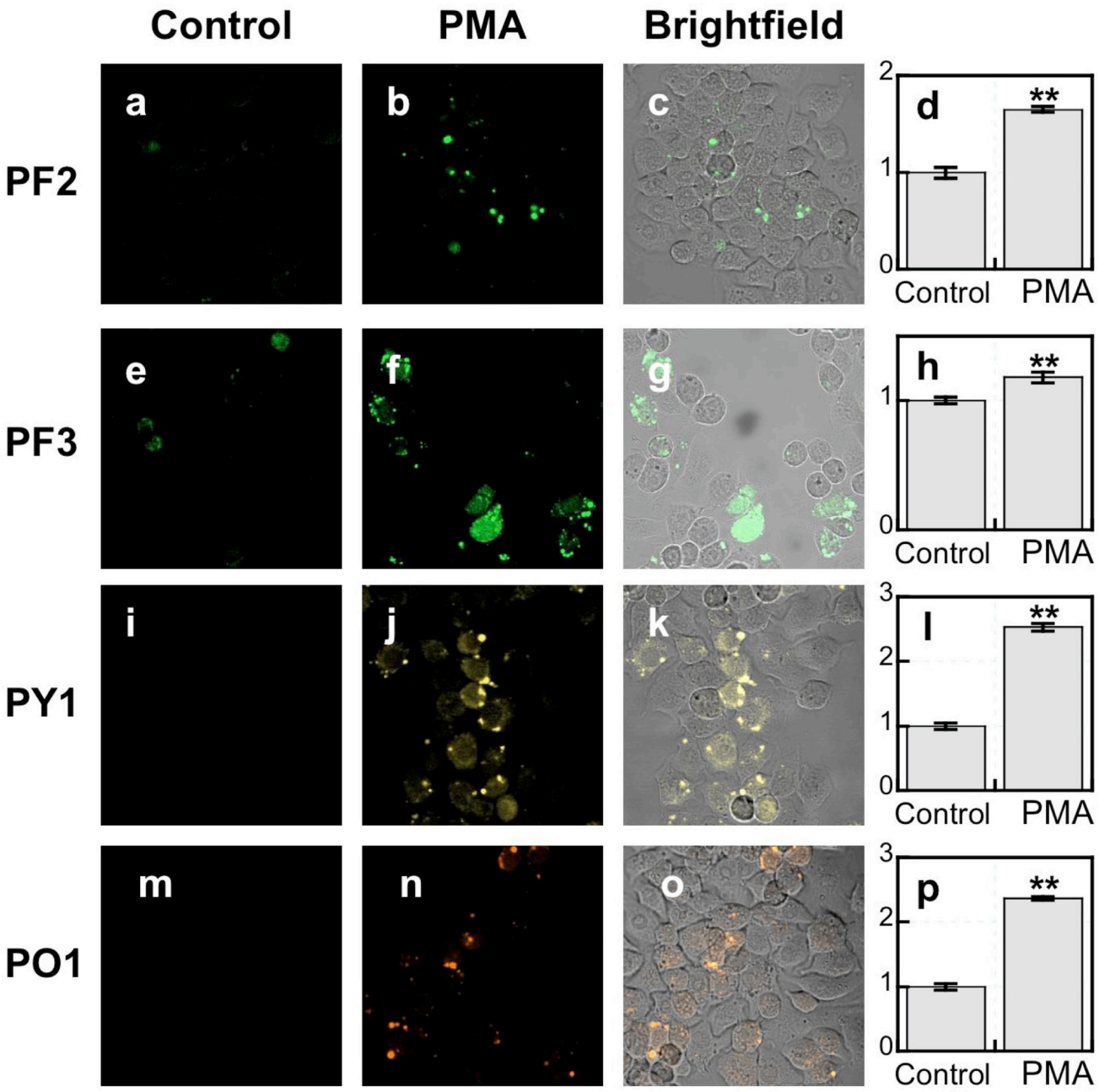

Figure 4.

Confocal fluorescence images of PMA-induced H_2O_2 production in live RAW264.7 macrophages with PF2, PF3-Ac, PY1 and PO1. Macrophages incubated with 10 μM PF2 for 60 min at 37 °C (a). Macrophages incubated with 10 μM PF2 for 60 min at 37 °C with 1 μg/mL PMA added for the final 40 min (b) with a brightfield overlay (c) and quantification (d). Macrophages incubated with 5 μM PF3-Ac for 60 min at 37 °C (e). Macrophages incubated with 5 μM PF3-Ac for 60 min at 37 °C with 1 μg/mL PMA added for the final 40 min (f) with a brightfield overlay (g) and quantification (h). Macrophages incubated with 5 μM PY1 for 60 min at 37 °C (i). Macrophages incubated with 5 μM PY1 for 60 min at 37 °C with 1 μg/mL PMA added for the final 40 min (j) with a brightfield overlay (k) and quantification (l).

Macrophages incubated with 5 μM PO1 for 60 min at 37 °C (m). Macrophages incubated with 5 μM PO1 for 60 min at 37 °C with 1 μg/mL PMA added for the final 40 min (n) with a brightfield overlay (o) and quantification (p). Data were normalized to controls and statistical analyses were performed with a two-tailed Student's *t*-test (n = 4). $^{**}P \leq 0.005$ and error bars are ± s.e.m.

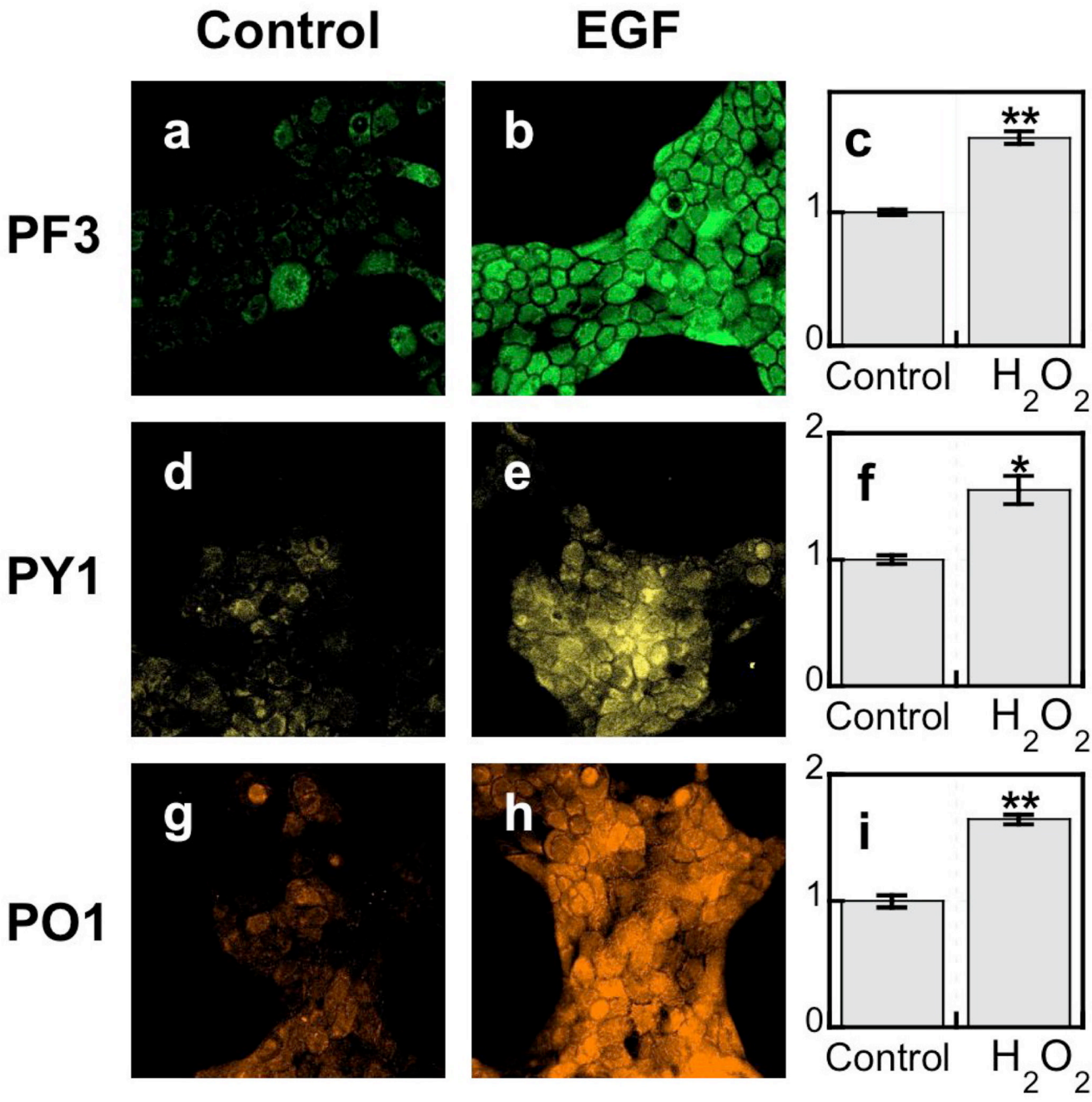

Figure 5.

Confocal fluorescence images of EGF-induced H_2O_2 in live A431 cells with PF3-Ac, PY1 and PO1. A431 cells incubated with 5 μM PF3-Ac for 60 min at 37 °C (a). A431 cells incubated with 5 μM PF3-Ac for 60 min at 37 °C with 500 ng/mL EGF added for the final 40 min (b) and quantification (c). A431 cells incubated with 5 μM PY1 for 60 min at 37 °C (d). A431 cells incubated with 5 μM PY1 for 60 min at 37 °C with 500 ng/mL EGF added for the final 40 min (e) and quantification (f). A431 cells incubated with 5 μM PO1 for 60 min at 37 °C (g). A431 cells incubated with 5 μM PO1 for 60 min at 37 °C with 500 ng/mL EGF added for the final 20 min (h) and quantification (i). Data were normalized to controls and statistical

analyses were performed with a two-tailed Student's *t*-test (n = 4). *$P \leq 0.05$, **$P \leq 0.005$ and error bars are ± s.e.m.

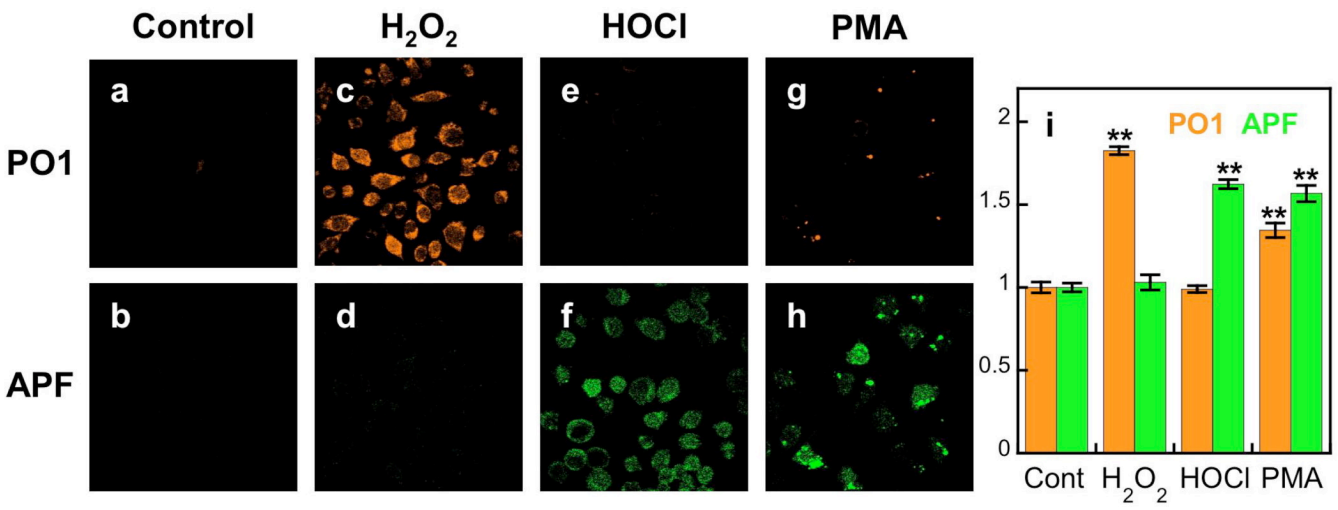

Figure 6.

Confocal fluorescence images of PMA-induced ROS production in live RAW264.7 macrophages with PO1 and APF simultaneously. Macrophages incubated with 5 μM PO1 and 5 μM APF for 40 min at 37 °C and imaged for PO1 (a) and APF (b). Macrophages incubated with 5 μM PO1 and 5 μM APF for 40 min at 37 °C with 50 μM H_2O_2 added for the final 20 min and imaged for PO1 (c) and APF (d). Macrophages incubated with 5 μM PO1 and 5 μM APF for 40 min at 37 °C with 100 μM HOCl added for the final 20 min and imaged for PO1 (e) and APF (f). Macrophages incubated with 5 μM PO1 and 5 μM APF for 40 min at 37 °C with 1 μg/mL PMA added for the final 20 min and imaged for PO1 (g) and APF (h). Quantification of a–h (i). Data were normalized to controls and statistical analyses were performed with a two-tailed Student's *t*-test (n = 4). $^{**}P \leq 0.005$ and error bars are ± s.e.m.

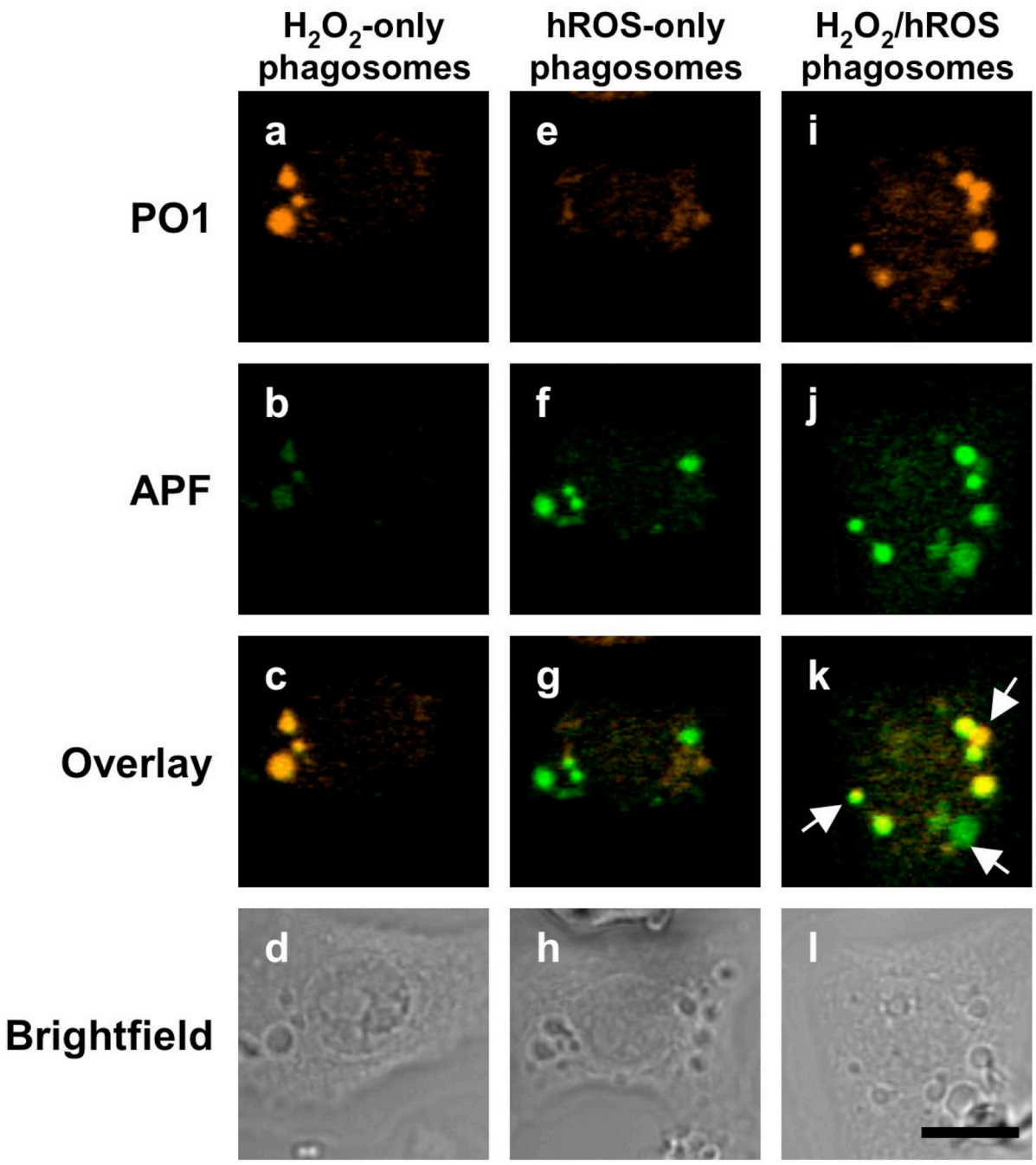

Figure 7.

Confocal fluorescence images of different types of phagosomes in live RAW264.7 macrophages distinguished by PO1 and APF. A macrophage producing mostly H_2O_2 as shown by the PO1 signal (a), APF signal (b), overlay (c) and brightfield (d). A macrophage producing mostly hROS as shown by the PO1 signal (e), APF signal (f), overlay (g) and brightfield (h). A macrophage producing a mixture of H_2O_2 phagosomes, hROS phagosomes, and H_2O_2 and hROS phagosomes. as shown by the PO1 signal (i), APF signal (j), overlay (k) and brightfield (l). 10 μm scale bar shown.

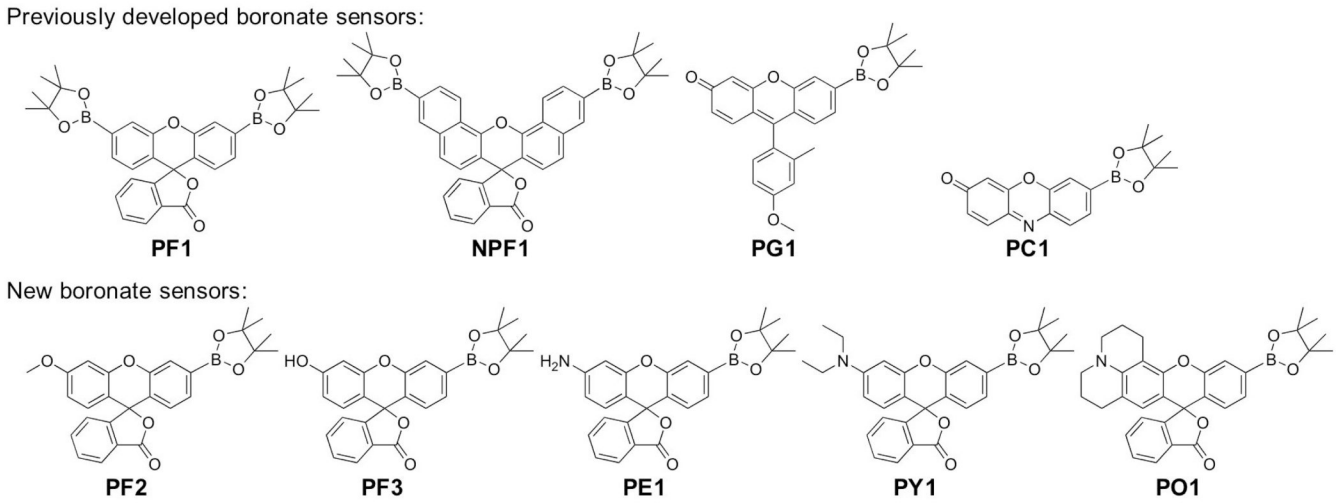

Scheme 1.
Boronate-based H_2O_2-specific fluorescent indicators.

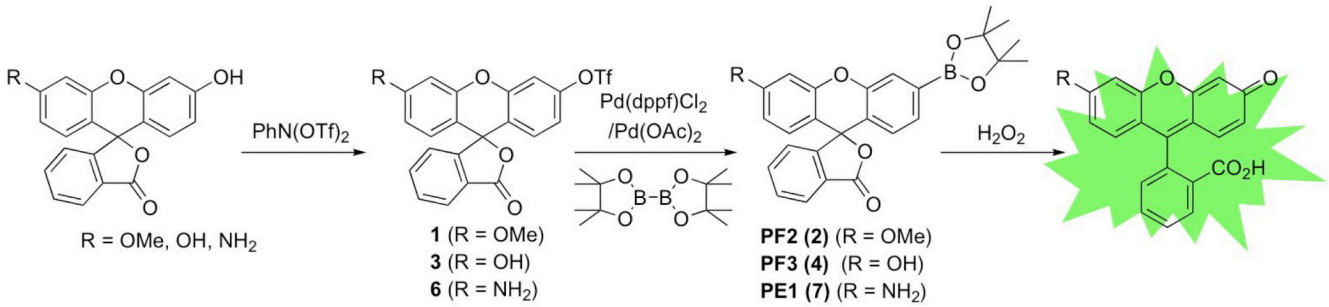

Scheme 2.
Synthesis and activation of PF2, PF3, and PE1.

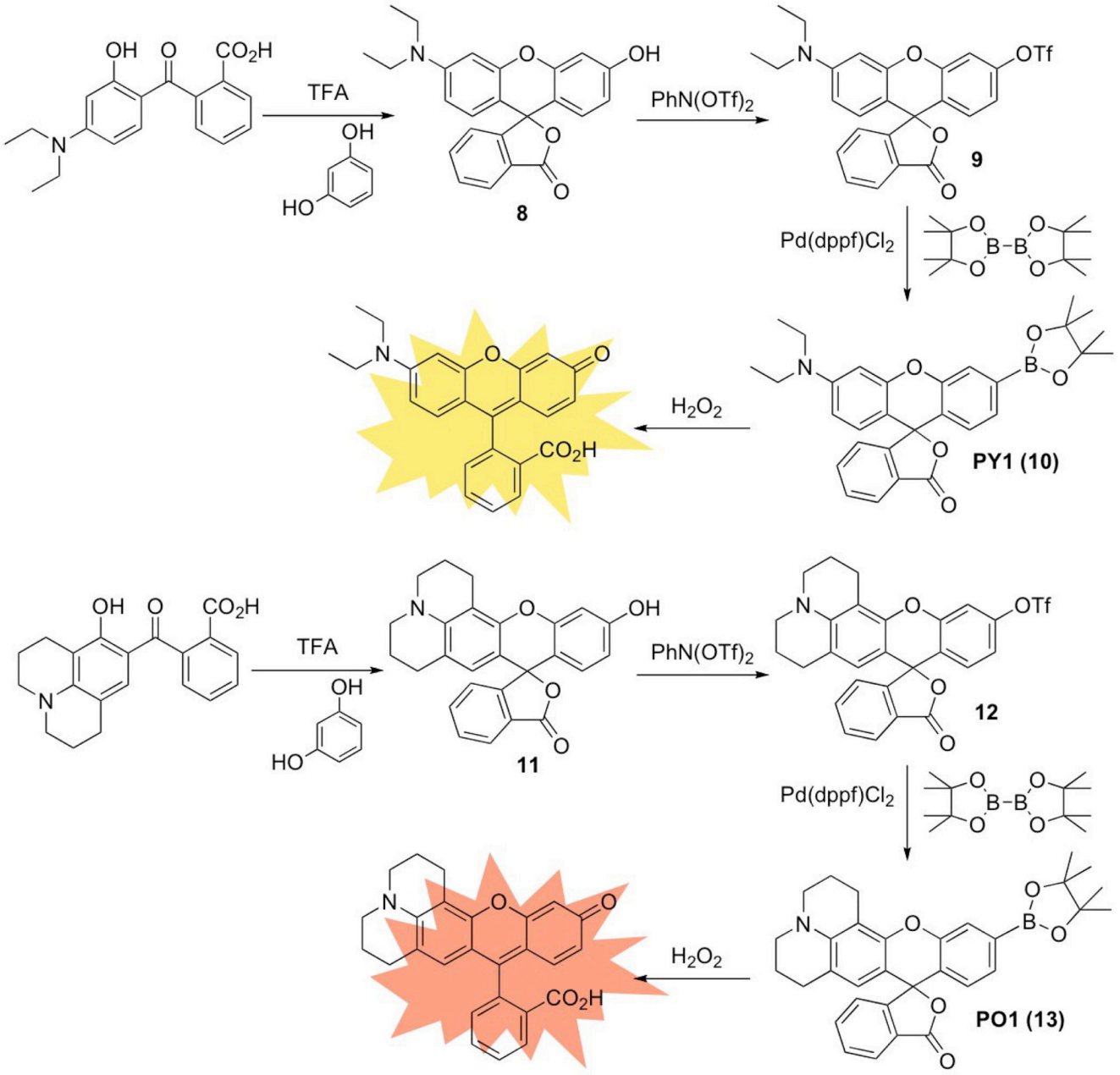

Scheme 3.
Synthesis and activation of PY1 and PO1.

Table 1

Spectroscopic properties of PF2, PF3, PE1, PY1, and PO1 acquired at 25 °C in 20 mM HEPES, pH 7. Fluorescein reported in 0.1 M NaOH.[104]

	Boronate-form				Phenol-form				
	λ_{abs} (nm)	ε ($M^{-1}cm^{-1}$)	λ_{em} (nm)	ϕ	λ_{abs} (nm)	ε ($M^{-1}cm^{-1}$)	λ_{em} (nm)	ϕ	k (× $10^{-3}s-1$)
PF2	n/a	n/a	n/a	n/a	475	28600	511	0.27	4.7 (1)
PF3	454	24000	521	0.10	492	88000	515	0.94	3.8 (1)
PE1	480	16400	519	0.30	491	51200	514	0.93	8.1 (1)
PY1	494	16200	558	0.01	519	48900	548	0.12	3.7 (1)
PO1	507	13900	574	0.07	540	29300	565	0.46	5.2 (1)